Impacts of Large-Scale Circulation on Urban Ambient Concentrations of Gaseous Elemental Mercury in New York, USA

Huiting Mao[1†], Dolly Hall[2], Zhuyun Ye[1], Ying Zhou[1], Dirk Felton[3], and Leiming Zhang[4]

[1]Department of Chemistry, State University of New York College of Environmental Science and Forestry, Syracuse, NY 13210
[2]Department of Atmospheric and Oceanic Science, University of Maryland, College Park, MD 20742
[3]Bureau of Air Quality Surveillance, Division of Air Resources, New York State Department of Environmental Conservation, Albany, NY 12233
[4]Air Quality Research Division, Science and Technology Branch, Environment and Climate Change Canada, Toronto, M3H 5T4, Canada

[†]Correspondence to: hmao@esf.edu

Abstract

The impact of large-scale circulation on urban gaseous elemental mercury (GEM) was investigated through analysis of 2008 – 2015 measurement data from an urban site in New York City (NYC), New York, USA. Distinct annual cycles were observed in 2009-2010 with mixing ratios in warm seasons (i.e. spring-summer) 10-20 ppqv (~10%-25%) higher than in cool seasons (i.e. fall-winter). This annual cycle was disrupted in 2011 by an anomalously strong influence of the US East coast trough in that warm season and was reproduced in 2014 associated with a particularly strong Bermuda High. US East coast trough axis index (TAI) and intensity index (TII) were used to characterize the effect of the US East coast trough on NYC GEM especially in winter and summer. The intensity and position of the Bermuda High appeared to have a significant impact on GEM in warm seasons. Regional influence on NYC GEM was supported by the GEM-carbon monoxide (CO) correlation with r of 0.17-0.69 ($p \sim 0$) in most seasons. Interannual variations were found in simulated regional and local anthropogenic contributions, averaged at ~75% (67%-83%) and 25% (17%-33%), respectively, to wintertime NYC anthropogenically induced GEM concentrations. Results from this study suggest the possibility that the increasingly strong Bermuda High over the past decades could dominate over anthropogenic mercury emission control in affecting ambient concentrations of mercury via regional build-up and possibly enhancing natural and legacy emissions.

1. Introduction

Atmospheric mercury (Hg) is a prevailing pollutant that has global consequences for both human and ecosystem health, and hence Hg emission control is imperative. Mercury in the atmosphere is operationally defined in three forms, gaseous elemental mercury (GEM), gaseous oxidized mercury (GOM), and particulate-bound mercury (PBM). Total gaseous mercury (TGM) is the sum of GEM and GOM. The most abundant of these three forms is GEM with a lifetime of 0.5 - 1 year (Driscoll et al., 2013) and mixing ratios on the order of hundreds of parts per quadrillion (ppqv) (~ a few ng m^{-3} at 1 ng m^{-3} = 112 ppqv in a standard atmosphere of 0°C and 1013.25 hPa; unit conversion was done in a standard atmosphere hereafter) compared to GOM and PBM with lifetimes of hours to weeks and mixing ratios often on the order of single ppqv (~ a few pg m^{-3}).

The median concentration of TGM/GEM in global continental remote areas was 1.6 ng m^{-3} (180 ppqv) estimated from a large body of measurement studies (Mao et al., 2016), and the background concentration of GEM in the Northern Hemisphere was 1.5 – 1.7 ng m^{-3} (168 – 190 ppqv) (Lindberg et al., 2007). Urban concentrations of GEM/TGM in the U.S. varied over 0.05 – 324 ng m^{-3} (5.6 – 36288 ppqv) (Mao et al., 2016). In comparison, urban concentrations and their temporal variability were larger than rural, remote, and high elevation concentrations in the Northern Hemisphere (e.g., Kim and Kim, 2001; Feng et al., 2003; Denis et al., 2006; Liu et al., 2007; Peterson et al., 2009; Sprovieri et al., 2010; Zhu et al., 2012; Lan et al., 2012, 2014; Chen et al., 2013; Civerolo et al., 2014; Fu et al., 2015; Brown et al., 2015; Mao et al., 2016 and references therein) owing to numerous controlling factors including anthropogenic and legacy emissions, deposition, meteorology, transport, and atmospheric chemistry (Mao et al., 2016).

Over the United States measurements from the Atmospheric Mercury Network (AMNet)

sites, located in urban, suburban, rural, and remote areas, suggested that monthly median GEM mixing ratios varied from 148 to 226 ppqv (~1.32 to 2.02 ng m^{-3}) with urban values at the higher end of the range (Lan et al., 2012). Urban ambient atmospheric TGM/GEM concentrations in Canada on average ranged over 1.7 – 4.5 ng m^{-3} (190 – 504 ng m^{-3}) (Mao et al., 2016; reference therein). Urban GEM/TGM concentrations in Asia could be an order of magnitude larger than those in the U.S., Canada, and Europe (Mao et al., 2016; references therein). Many studies identified local sources as a predominant factor controlling urban ambient concentrations (Gabriel et al., 2005; Lyman and Gustin, 2009; Wang et al., 2013; Feng et al., 2003; Fang et al., 2004; Zhu et al., 2012; Hall et al., 2014; Seo et al., 2016; Kim et al., 2016). In some urban locations nighttime daily maximums and spring-summer annual peaks were attributed to local and regional sources followed by boundary layer dynamics and meteorological conditions (Liu et al., 2007; Cheng et al., 2009; Liu et al., 2010; Nair et al., 2012; Zhu et al., 2012). Surface emissions were also suggested to play a major role in warm season annual maximums (Denis et al., 2006; Zhu et al., 2012). Some sites experienced early morning daily maximums with the strongest diurnal variation in summer, due possibly to local anthropogenic sources and surface emissions (Stamenkovic et al., 2007; Peterson et al., 2009). Wintertime annual maximums were attributed to probably more coal combustion to produce energy for space heating, less oxidation of GEM (Stamenkovic et al., 2007) and periods of cold and stagnant air probably leading to build-up of pollution and more Hg evasion prompted by wet conditions (Peterson et al., 2009). Temporal variations of GEM concentrations could be attributed to the combined influence of environmental variables, anthropogenic sources, photochemistry, and regional transport (Xu et al., 2014).

Some studies suggested that regional sources dominated over local ones in contributing to

urban ambient Hg concentrations (e.g., Liu et al., 2007; Kim et al., 2013; Engle et al.; 2010; Xu et al., 2014; Hall et al., 2014). On interannual time scales, the impact of regional transport, in comparison to local sources, could vary greatly due to large variability in atmospheric circulation and subsequently affect urban ambient concentrations very differently. Additional emission control is anticipated in the future associated with the Mercury and Air Toxics Standards (MATS) rule and the United Nations Environment Program (UNEP) international Minamata Treaty (Selin, 2014). To regulate future emissions, it is important to understand and quantify contributions of local versus regional sources to urban ambient concentrations. The objective of this paper is to examine the seasonal, annual, and interannual variability of GEM in the Bronx Borough of New York City (NYC) and its relation with large-scale circulation, and the contributions of local and regional sources to NYC ambient GEM concentrations.

2. Data and Approaches

2.1 Site description

The site discussed herein is maintained by the New York State Department of Environmental Conservation (NYSDEC) as a part of AMNet under the National Atmospheric Deposition Program (NADP) and the National Toxic Network (NTN). The monitoring site is located on the rooftop of the Pfizer Plant Resource Laboratory on the northern edge of the New York Botanical Garden in the north Bronx (40°52′05″N, 73°52′42″W; USEPA site ID 36-005-0133). The height of the measurement point is about 9 m from ground surface, and winds arriving at the location are not significantly obstructed by immediate surroundings. The 100 ha New York Botanical Garden is surrounded by highways and mixed residential/commercial areas. New York City is a metropolitan area with a >19 million population, and the region has a long manufacturing, petrochemical, and industrial legacy that includes contamination from Hg and

other toxic compounds. The Bronx site is also downwind of many regional sources (Fig. 1). Continuous measurements of meteorological variables and trace gas and toxic air pollutants are conducted at this site. Additional details on the site can be found on the NYSDEC website (http://www.dec.ny.gov/docs/air_pdf/2017 plan.pdf).

2.2 Measurement data

GEM was measured every 5 minutes using a Tekran (Toronto, ON) model 2537B (August 27, 2008 through October 24, 2013) or 2537X (October 25, 2013 onward) cold vapor atomic fluorescence (CVAF) analyzer with a nominal detection limit of <0.1 ng m^{-3} (~11.2 ppqv). The instrument was calibrated daily with an internal permeation source. The Tekran system was operated according to standard operating procedures from the NADP's AMNet. The AMNet site liaison performs annual site visits, which include manual injections to verify the internal permeation source, and is responsible for quality assurance of the data (Civerolo et al., 2014). Additional details can be found in Landis et al. (2002) and Gay et al. (2013).

Measurement data of sulfur dioxide (SO_2), nitrogen dioxide (NO_2), carbon monoxide (CO), temperature, wind direction, and wind speed were averaged hourly. The SO_2 measurements were taken using a TEI 43C and a 43i TLE instrument using pulsed fluorescence. The NO_2 measurements were taken using a TEI 42C instrument using conversion on a heated molybdenum catalyst followed by chemiluminescence. It is acknowledged that this method is not specific to NO2 and suffers from interferences due to other oxides of nitrogen. However, in this dense urban area with ample fresh anthropogenic emissions, this artifact is relatively small in an absolute sense since nitric oxide (NO) and NO_2 account for a substantial fraction of total reactive nitrogen. CO was measured by a TEI 48C and an API 300EU instrument using reference method 054 with non-dispersive infrared absorption. The technical details of the

deployment of these instruments are given by the NYSDEC at www.dec.ny.gov/chemical/8541.html and in the 2016 Annual Monitoring Network Plan (www.dec.ny.gov/docs/air_pdf/2016plan.pdf).

2.3 HYSPLIT Dispersion model description, configuration, and simulation scenarios

The impact of regional and local anthropogenic sources was simulated using the NOAA Hybrid Single Particle Lagrangian Integrated Trajectory model (HYSPLIT) dispersion version (Draxler and Hess, 1997, 1998; Draxler, 1999; Stein et al., 2015) for the winters and summers of 2009 – 2015. HYSPLIT was driven by the EDAS 40 km model output over a domain extending westward to OH, southward to northern VA, and northward to include New England (Fig. 10a). The model was run in the forward mode for 120 hours for each day of a season.

The dispersion of a pollutant is calculated by assuming a fixed number of particles being advected about the model domain by the mean wind field and spread by a turbulent component, and by assigning certain mass to a particle, emissions are incorporated in the model (Stein et al., 2015). There were a total of 522 counties within the domain reporting Hg emissions that were extracted from the US Environmental Protection Agency (EPA)'s National Emission Inventory (NEI) 2011 (https://www.epa.gov/air-emissions-inventories/2011-national-emissions-inventory-nei-data). Note that the total emissions of Hg were treated as 100% GEM emissions. The US EPA's NEI documents emissions on a county, annual basis. For model simulations the EPA emission amount for each county was broken down to an hourly rate by the annual emission amount divided by (365x24). Two emission scenarios were designed. One scenario included emissions from all the 522 counties, and the other scenario excluded emissions from the five boroughs in NYC. Output of Scenario #2 quantified the effect of anthropogenic emissions outside of NYC (denoted as regional sources) on NYC ambient GEM concentrations due to long

range transport only. The difference in NYC GEM concentrations between the two scenarios was used to approximate the effect of local sources only on NYC GEM concentrations.

2.4 Large-scale circulation analysis

In the analysis of the US East coast trough, the trough axis index (TAI) and trough intensity index (TII) defined by Bradbury et al. (2002) were used to quantify the position and intensity of the US East coast trough. The seasonal TAI quantifies the mean longitudinal position of the quasi-stationary midtropospheric East Coast trough. The TAI domain extends from 120°W to 30°W and the southern to northern boundaries ranged from 40°N to 50°N. The TAI index was calculated by averaging the longitudinal positions (Lon) of the minimum 500-hPa heights (H_{min}) observed at each of the four latitudinal steps (j=40°, 42.5°, 45°, and 47.5°N) within the index range, to produce a practical index in longitudinal units (relative to the prime meridian):

$$TAI = \text{average } [Lon(H_{min})_j]$$

The TII is an estimate of wave amplitude at 42.5°N and is the mean height change at the 500-hPa surface from equal distances east and west of the East Coast trough axis. It was calculated:

$$TII = \{[(H_{min})_i - H_{i+30°}) + [(H_{min})_i - H_{i-30°}]\}/2$$

The more negative TII is, the stronger the influence of the US East coast trough would be. The 2.5° x 2.5° reanalysis data from the National Center of Environmental Protection/National Center of Atmospheric Research were used to calculated seasonal average TAI and TII. Additional details about TAI and TII can be found in Bradbury et al. (2002).

3. Results and Discussion

3.1 General Characteristics of Diurnal, Seasonal, and Interannual Variation

Annual cycles of 2009, 2010, and 2014 displayed larger GEM mixing ratios (>the 75th

174 percentile value of the entire study) during the warm seasons (summer-spring) than the cool
175 seasons (fall-winter) (Fig. 2; Table 1), in agreement with previous urban site studies (Denis et al.,
176 2006; Liu et al., 2007; Zhu et al., 2012; Zhang et al., 2013; Civerolo et al., 2014). The pattern of
177 such annual cycles was evidenced in >20% (<10%) of the warm (cold) season in 2009 and 2010,
178 and 67% (31%) of the warm (cold) season in 2014 experiencing larger GEM mixing ratios
179 (Table 1). However, this pattern was not reproduced in 2011 and 2012, where the frequency of
180 occurrence of larger GEM values was either comparable between the two seasons or slightly
181 higher in the cold season.

182 Three salient features were evident in the interannual variation of a range of percentile
183 mixing ratios of GEM (Fig. 3; Table 1). First, the 2009 – 2010 cool season percentile values of
184 GEM were the lowest of all cool seasons. Second, the 2011 warm season percentile values were
185 the lowest of all warm seasons, even lower than in the cool season of the same year, not
186 reproducing the 2009 and 2010 annual cycles. Third, the 2014 and 2015 seasonal percentile
187 values were mostly the highest of the study period and for the first time since 2011, warm season
188 values exceeded the cool season ones reproducing the 2009 and 2010 annual cycles.

189 The most pronounced diurnal cycles occurred in summer, as shown in seasonal average
190 diurnal cycles in Figure 4, with a peak between 02:00 and 06:00 UTC and a minimum between
191 10:00 and 16:00 UTC, which is consistent with previous studies for urban locations (e.g. Denis et
192 al., 2006; Liu et al., 2007; Zhu et al., 2012; Lan et al., 2012). In summers of 2009 – 2012, the
193 daily maximum was ~170-190 ppqv and the daily minimum ~140-160 ppqv. The diurnal
194 amplitude, defined as the difference between the daily maximum and minimum, was up to ~50
195 ppqv in summer, ~20 ppqv in fall and spring, and <10 ppqv in winter.

196 During 2008 – 2013, the cool seasons experienced much larger interannual variability of

GEM than the warm seasons did, whereas in 2014 and 2015 GEM concentrations were elevated significantly above other years in all seasons (Fig. 4). Over 2008 - 2013, the largest interannual variability up to ~40 ppqv difference was observed between the lowest GEM mixing ratios in fall 2009 and largest in fall 2012, whereas springs and summers experienced much less interannual variability except spring and summer 2011, as aforementioned, that saw the lowest GEM mixing ratios, ~ 20 ppqv lower than all other warm seasons.

3.2. Interannual Variation of Cool Season GEM

The 2009 – 2010 cool season exhibited the lowest percentile values whereas most of winter 2014 and cool season 2014-2015 percentile values were the highest of the study period (Table 1; Fig. 3). The difference in percentile values between the two cool seasons ranged from 30-40 ppqv in the 25^{th} and median values to 37 – 67 ppqv in the 90^{th} percentile value. The possible effect of anthropogenic emission changes on those interannual variations in GEM concentrations was the very first to be examined. EPA national emission inventories showed a 13% decrease from 2008 (31810 kg) to 2011 (27695 kg), and then an increase of 2% to 2014 (28270 kg) in total emissions from the Eastern US, including states east of the Mississippi River, of which NYC emissions increased from 125 kg in 2008 to 145 kg in 2011 and to 199 kg in 2014 (https://www.epa.gov/air-emissions-inventories/2014-national-emissions-inventory-nei-data). Using an average PBL height of 1000 m over the Eastern US (the surface area for the Eastern US is 2.483×10^{12} m^2), a decrease of 4115 kg from 2008 to 2011 emissions was converted to a total decrease of 200 ppqv over all days of the three years and averaged at a decreasing rate of 0.2 ppqv d^{-1}, and an increase of 575 kg from 2011 to 2014 emissions was converted to a rate of ~0.03 ppqv d^{-1}. The potential change in NYC atmospheric concentrations were estimated to be ~3 ppqv d^{-1} from the 2008 – 2011 NYC emission increases alone and ~6 ppqv d^{-1} from the 2011

220 – 2014 increase. The potential changes in ambient concentrations caused by the regional
221 emission decrease/increase were negligible compared to the observed interannual difference.
222 Those caused possibly by NYC emission increases could be significant but appeared to be
223 inconsistent with the changes in ambient concentrations in two ways. First, from 2010 to 2011
224 NYC emissions increased and yet summertime ambient concentrations decreased by 10 ppqv
225 throughout the seasonal averaged diurnal cycle (Fig. 4). Second, if the residence time of emitted
226 GEM was 1 day, the total increase in ambient mixing ratio would be 6 ppqv d^{-1} due to
227 anthropogenic emission increases and would be even smaller spreading throughout the day,
228 which was negligible compared to the ~60 ppqv increase observed in the spring 2011 seasonal
229 average diurnal cycle compared to the spring 2014 one (Fig. 4). The contribution from the NYC
230 anthropogenic emissions to ambient GEM was further demonstrated using HYSPLIT simulations
231 in Section 5.

232 Legacy and natural emissions could be another driver for the observed interannual
233 variations in GEM. However, seasonal mean temperature and GEM from the Bronx location
234 were not found to be correlated, which suggested that the effect of changes in legacy and natural
235 emissions on ambient GEM might not be dominant. In addition, using Zhang et al. (2016)'s
236 estimated annual natural and reemissions 9.4 to 13.0 μg m^{-2} for the Bronx site during 2009-2014,
237 the maximum year-to-year change was calculated to be ~1 ppqv d^{-1} assuming an average
238 planetary boundary layer (PBL) height of 1000 m. This change alone could not explain the
239 observed interannual variations. It alludes to the potential effect of *regional* legacy and natural
240 emissions as well as chemistry, which needs to employ modeling tools and is beyond the scope
241 of this study. Here, it was hypothesized that atmospheric circulation was one predominant factor
242 contributing to the observed interannual variation in Bronx ambient GEM concentrations.

To validate this hypothesis, circulation patterns were examined first using the Bronx site wind data. In falls 2008, 2009, 2011, and 2013, wind came from all four quadrants with comparable frequency ranging over 15% - 30% of the season, whereas in fall 2010 the northwesterly (270°-360°) was more frequent (37%), and the northeasterly (0°-90°) became predominant (~50 – 74%) in falls 2012 and 2014 (Fig. 5a). The winters experienced northwesterly winds (270°-360°) more often ranging from ~40% to 65% of the season with the exception of winter 2015 when a little below 40% of the season on par with southwesterly wind (180°-270°) (Fig. 5a). Wind speed was averaged seasonally for the four wind quadrants (Fig. 5b). Northwesterly wind (270°-360°) was the strongest (>3 m s^{-1}) in winters and springs of 2009 – 2013 and was reduced to ~ 2 m s^{-1} in 2014 and 2015. Southwesterly (180°-270°) wind hovered around 2 m s^{-1} in the cool seasons except 2009-2010 when it was lowered to 1 m s^{-1}. Wind speed in the two easterly quadrants (0°-180°) was comparable varying over 1 – 2 m s^{-1} except that in spring 2013 it reached 2.5 m s^{-1} and was particularly low (0.5 m s^{-1}) in the 2014 cool season.

Since Hg anthropogenic sources are mostly concentrated to the west, southwest, south, and northeast of the Bronx site with much fewer sources to the northwest (Fig. 1), GEM mixing ratios would vary expectedly corresponding to air masses arriving from different directions. This was clearly suggested by mixing ratios of GEM averaged seasonally for the four wind quadrants (Fig. 5c). Generally, seasonally averaged GEM mixing ratios were larger by ~20-50 ppqv in the two southerly than those in the northerly quadrants. Overall, in addition to local emissions, interannual variability in the origin of the air masses reaching Bronx appeared to cast significant influence on the ambient concentrations of GEM in the city. This argument was strongly supported by SO_2 values in the four wind quadrants (Fig. 5d). Consistent with GEM (Fig. 5c), southwesterly (180°-270°) wind brought in air masses with the highest SO_2 levels in 2008 –

2011, especially in winter reaching 13-14 ppbv, followed by half the values in winters of 2012 – 2015. In contrast, the SO_2 mixing ratios were close in the other three wind quadrants. One difference between the variation patterns of GEM and SO_2 in the four wind quadrants was that air masses from the southeast appeared to be also rich in GEM, whereas SO_2 in air from the southeast was low, close to that from the northwest and northeast. One confounding factor for this difference could be due to the ocean being a major of source of GEM, and also the only landmass southeast of the Bronx is Long Island, with limited major polluters.

Two cases, the lowest percentile values in the 2009–2010 cool season and the highest in 2014-2015, were used to elaborate on this point. What was most striking about the 2009 – 2010 cool season was very low frequency (14%) of wind from the southwesterly quadrant (180°-270°) in fall 2009 and the largest frequency of wind from the northwesterly quadrant (67%, 270°-360°) in winter 2010 combined with nearly the lowest wind speed ($\leq$ 1 m s^{-1}) in the three quadrants (0°-270°) (Figs. 5a-c). This indicates that the particularly low mixing ratios in the cool season of 2009 – 2010 were likely caused by over 4 times more frequent influx of relatively cleaner Canadian air masses and slowest southerly flow of more polluted air.

The second case is winter 2014 when GEM averaged in the four wind quadrants reached the maximums of all time respectively (Fig. 5c). Coincidently the frequency of wind from the northwesterly quadrant (270°-360°) was nearly the lowest of all cool seasons barely reaching 40% of the season compared to up to 67% in winter 2010 (Fig. 5a). Meanwhile, the frequency of wind from the southwesterly quadrant (180°-270°) reached a high of 34% of all cool seasons, and the wind speed of ~2 m s^{-1} was comparable to the northwesterly. This is a strong indication of arrival of air masses rich in GEM originating from the heavy emitters in the Northeastern U.S. Urban Corridor via flow nearly as frequent and as fast as the relatively clean northwesterly.

289 Winter 2015 showed similar wind patterns, also coincided with high GEM concentrations.
290 Such variations in wind direction and speed at the Bronx site can be better understood in
291 the context of large-scale circulation. The climatological 500 hPa geopotential height (GPH)
292 (1980-2010) for cool seasons during 1980-2010 exhibited the US East coast trough centered over
293 coastal southeastern Canada extending southwestward over the Eastern US (Fig. 6a). All cool
294 seasons experienced variations of this pattern except cool seasons 2009-2010 and 2013-2014 that
295 appeared to be anomalous (Figs. 6b and 6c). Specifically the trough in winter 2010 shifted
296 eastward farthest out over the ocean and was the weakest, evidenced in the maximum TAI
297 (62°W) and nearly the least negative TII value (-80 m) (Fig. 6d). In contrast, the trough in
298 winter 2014 was situated the farthest over land and the strongest of all winters, backed by the
299 most negative TAI (85°W) and nearly the most negative TII value (-201 m) (Fig. 6d) . This
300 suggested that in winter 2010 the Northeast US was most frequently under the influence of air
301 masses from higher latitudes via flow on the backside of the US East coast trough whereas much
302 less so due to the East U.S. positioned near the axis to the front of the trough in winter 2014.
303 This was further clearly reflected in the maps of sea level pressure (SLP) for the two winters.
304 The unusual winter 2010 circulation was signified by northerly gradient flow (Fig. 6f) from the
305 backside of the Icelandic Low, which shifted toward the south and west near Newfoundland
306 compared to its 1980-2010 climatological position right between and below Greenland and
307 Iceland (Fig. 6e). This indicated predominant transport of relatively clean air from Canada
308 combined with strong ventilation of continental pollution, likely leading to the least polluted air
309 in winter 2010 of all 7 winters. In contrast, in winter 2014 NYC appeared to be on the periphery
310 of high pressure systems in predominantly slow northwesterly and southwesterly flow regimes
311 (Fig. 6g). This explains the least frequent, lowest wind speed in the easterly wind quadrants

during winter 2014 (Fig. 5b), which is conducive to regional build-up of air pollution, resulting in the highest mixing ratios of GEM of all winters. More evidence was shown in Section 6 using modeled contributions to NYC ambient concentrations from local versus regional anthropogenic sources.

3.3 Interannaul Variation of Warm Season GEM

3.3.1 Annual maximums in warm seasons of 2009 and 2010

The annual cycles of GEM at the Bronx site in 2009 and 2010, with larger values in spring and summer (Table 1; Figs. 2 and 3), is consistent with measurements from some urban and industrial locations in the literature (Lindberg and Stratton, 1998; Liu et al., 2007; Zhu et al., 2012; Xu et al., 2014). Lindberg and Stratton (1998) and Liu et al. (2007) attributed such annual cycles to local anthropogenic sources, while Zhu et al. (2012) and Xu et al. (2014) speculated reemission from soils to be a potential dominant factor. In NYC, impervious surfaces comprise 95% of the total land surface (Adler and Tanner, 2013), which, considering local sources alone, makes reemission of Hg from soils much less significant than anthropogenic emissions from the area. Indeed no correlation between seasonal temperature and GEM was found for the Bronx site (not shown). It thus seemed unlikely that NYC legacy emissions contributed to the 2009 and 2010 annual cycles. The impact of regional vs. local anthropogenic sources on NYC GEM concentrations was studied in Section 3.5, and quantifying the impact of *regional* natural and legacy emissions calls for a regional modeling approach, which is beyond the scope of this study. Here we focused on the potential impact of large-scale circulation on NYC GEM concentrations.

In the warm seasons, Bronx was on the periphery of the Bermuda High (Figs. 7c,f), where usually lower wind speed prevailed. This is consistent with the annual cycle of wind speed shown in Figure 5b, with wind mostly lower in spring-summer and higher in fall-winter

conducive to regional pollution build-up, which could explain why Bronx saw larger peaks of GEM in the warm season than in the cool season.

3.3.2 Lowest GEM in warm season 2011 and highest in 2014 & 2015

In examining wind in the warm season 2011, what stood out was that Bronx experienced significantly increased frequency (37%) of northeasterly wind of ~2 m s^{-1} in spring and decreased frequency of (20%) of northwesterly wind in summer compared to the spring and summer in 2009 and 2010 (Fig. 5a). In summer 2014 nearly 80% of the season had northeasterly wind (0°-90°) and there was unusually weak wind (~1 m s^{-1}) in all four wind quadrants (Figs. 5a,b), which suggested calm conditions. In the warm season of 2011GEM concentrations in the northeasterly wind quadrant were averaged ~145 ppqv, up to ~ 20 ppqv lower than that in the most polluted southerly quadrants (Fig. 5c). In contrast, springs of 2014 and 2015 GEM in the northeasterly quadrant was averaged 200 and 192 ppqv, respectively, equally large or even larger than GEM in the other three quadrants (Fig. 5c). The unusually high concentration was an indication of build-up under calm conditions.

The anomalously increased occurrence of northeasterly wind in summer 2011 indicated unusual circulation. Compared to the 1980-2010 climatology, the 500 hPa GPH in spring 2011 showed the weakest US East coast trough of all springs (Fig. S1), evidenced in the westernmost trough axis position (TAI = 108°W) and the smallest intensity (TII = -27 m) of all springs (Fig. 7a). The 500 hPa GPH in summer 2011 suggested the strongest US East coast trough (TII = -87 m) and the second easternmost trough axis position (TAI = 66°W) of all summers (Fig. 7b; Fig. S2). This suggests that the Northeast U.S. in summer 2011 was frequently under significant influence of the backside of the trough, i.e. sweeping air flow from higher latitudes subsiding to the surface in midlatitudes.

Near the surface, the 1980-2010 SLP climatology suggested that in spring NYC was situated in the gradient flow of the Bermuda High and a trough from the Icelandic Low (Fig. 7c), conducive to transport of emissions from upstream source regions such as upstate New York, Ohio (OH) and Pennsylvania (PA), while in summer under the influence of the Bermuda High favorable to regional build-up (Fig. 7f). However, in spring 2011, the trough of the Icelandic Low gave way to the Canadian High leaving NYC locked in a zone between the Canadian High and subtropical high (Fig. 7d), possibly cutting regional transport short in addition to strong subsidence of cleaner higher latitudinal air leading to the lowest concentrations of GEM of all springs. Similarly unusual was summer 2011 when NYC was under less influence of the Bermuda High than that of the US East coast trough unfavorable to regional build-up (Fig. 7g). These speculations appeared to be consistent with the fact that both seasons saw unusual equal chances of winds from the four quadrants (Fig. 5a) over Bronx and its surrounding areas.

The 500 hPa TAI and TII values (Figs. 7b) and the 500 hPa GPH map (Fig. S2) in summer 2011 suggested the strongest (TII = -87 m) and second easternmost (TAI=66°W) US East Coast trough. In comparison, summer 2014 (Fig. S2) saw the weakest US East Coast trough (TII = -44 m) of all summers, with its axis on average at 72°W, near the East Coast. This contrast indicates that summer 2011 experienced the weakest influence of the Bermuda High on the East Coast (Figs. 7e,h) of all summers during the study period, the polar extreme of the 2014 warm season. Corresponding to that, the spring and summer 2014 SLP maps (Figs. S3&S4) exhibited the Bermuda High ridge over the Eastern U.S. more north-extending than in other years, which is consistent with weak winds in all directions as shown in Fig. 5b. This dynamic situation led to regional build-up conducive to the highest GEM mixing ratios in all wind quadrants.

To be quantitative, domain (25°N-50°N, 95°W-70°W) average SLP, the number of grids with SLP exceeding 1014 hPa over the domain, the northernmost latitude, and westernmost longitude of the 1014 hPa isobar were examined to gauge the intensity and spatial extent of the influence of the Bermuda High. The domain average SLP and the number of grids with SLP>1014 hPa turned out to be best correlated (r=0.95, p=0.05; r=0.99, p=0.006) with summer season median GEM (Fig. 8). The lowest GEM in summer 2011 was associated with the weakest influence of the Bermuda High indicated by the lowest domain average SLP (1013 hPa) and least number (63) of grids with SLP> 1014 hPa of all summers. Meanwhile the US East Coast trough reached as far down south as North Carolina (Fig. S4), consistent with the most negative TII (-90 m) as aforementioned and shown in Fig. 7b. This indicates more widespread influence of relatively clean Canadian air on the Eastern US sweeping out the heavily polluted air in the region. One may argue that the positive correlation shown above appeared to be driven by the four points in summers 2009 – 2012 due to missing/unavailable data in summers 2013 and 2014. It should be noted that the increases in GEM started in winter 2014, consistently evidenced in measurements available through spring 2015 compared to all previous years (Fig. 3). Therefore, the large increase in the 2014 warm season was most likely not fortuitous, and more importantly such increases were consistent with the driving dynamical mechanisms as suggested in the large scale-circulation.

It should be noted that the seasonal median GEM values in the four wind quadrants exhibited trends largely consistent with those in the overall seasonal values (r=0.87 – 0.95, p ~0) (Fig. 5c). This suggests that changes in ambient mixing ratios occurred in air masses coming from all directions, whether they were from the relatively clean northwest and northeast, or the heavily polluted regions southeast and southwest of Bronx. A possible explanation is that the

lifetime of GEM is long enough for air from all wind directions to be regionally mixed. The fact that the GEM values in the two relatively more polluted quadrants exhibited excellent correlations with the overall values suggested that the trend in the ambient GEM mixing ratio was largely shaped by the variability of anthropogenic influence. Such influence may not necessarily be driven by changes in anthropogenic emissions but could be caused by strong ventilation or regional build-up of pollution as demonstrated in earlier discussions.

3.4 Relationships Between GEM and Anthropogenic Tracers

Correlations between Hg and several tracers (e.g., CO, SO_2, and NO_2) have been commonly used to identify Hg anthropogenic sources, source-receptor relationships, and/or emission ratios. The linear correlation between CO and GEM, especially in winter, in rural locations despite their different sources, reflects their emission ratios in regionally well-mixed air masses (e.g., Mao et al., 2008). At the Bronx site, seasonal GEM and CO were found to be correlated with r up to 0.69 (p~0) in all seasons over 2008 -2013, indicating significant, year-round *regional* influence, and the two were notably not or minimally correlated in all the seasons from winter 2014 through spring 2015. Over 2008 – 2010 and 2012 r^2 values of GEM-CO were larger in warm than in cold seasons with the maximums exceeding 0.40, and r^2 values remained high from winter 2011 through winter 2012 (Fig. 9). The slope value varied from the smallest (~0.02-0.03 ppqv $ppbv^{-1}$) in winters of 2009 – 2010 to the largest (0.21 ppqv $ppbv^{-1}$) in summer 2012 (Fig. 9), with the largest higher than the upper end of the range, 0.06 – 0.14 ppqv $ppbv^{-1}$, from rural southern New Hampshire (NH) during winters 2004 – 2007 (Mao et al., 2008). This was greatly different from the GEM-CO correlation in rural southern NH in winter only due to confounding factors such as legacy emissions and wet deposition in summer (Mao et al., 2008; Lombard et al., 2011). Bronx experiencing more significant GEM-CO correlation in warm

seasons indicated better regionally mixed air masses, influenced predominantly by anthropogenic emissions, than in cool seasons. This is consistent with the cool and warm seasonal circulation patterns as discussed in Sections 3.2 and 3.3, which is that in warm seasons NYC was predominantly under the influence of the subtropical high conducive to regional mixing and build-up of pollutants.

No correlation between GEM and CO over 2014 – 2015 could be due in part to the more dramatic emission reductions in CO than changes in GEM in the Eastern U.S. The high percentile values of CO at the Bronx site had been affected by anthropogenic emission reductions over the years, while the 10^{th} and 25^{th} percentile values (referred to as baseline CO in the literature) remained fairly constant in all seasons (Fig. S5). Zhou et al. (2017) suggested that baseline CO in Northeastern US rural areas was controlled by a multitude of factors including global biomass emissions, large-scale circulation, and cyclone activity. At the Bronx site, the low percentile value, close to regional baseline levels, was possibly determined by a range of factors, whose importance could have varied from year to year.

Unlike previous studies (e.g., Jen et al., 2013; Choi et al., 2013), GEM at the Bronx site was found poorly correlated with SO_2 while somewhat to moderately correlated with NO_2 (r = 0.13 – 0.71, p<0.0001) (Table 2), despite abundant sources co-emitting GEM, SO_2, and NO_2 locally and upwind. In addition to different lifetimes, different magnitude and timing of emission reduction implementations and source types of the three compounds could have affected their relation. Total Hg anthropogenic emissions in NYC were increased by 16% from 2008 to 2011, mainly in miscellaneous non-industrial NEC and waste disposal emissions, and further increased by 37% from 2011 to 2014 primarily in fuel combustion. As aforementioned, emissions of Hg in the Eastern U.S. decreased by 13% from 2008 to 2011 and increased by 2%

from 2011 to 2014. In contrast, total SO_2 emissions in NYC decreased steadily by 30% from 2008 to 2011 followed by a further decrease of 43% to 2014, while over the Eastern U.S decreased by 48% from 2008 to 2011 and furthered by another 29% decrease in 2014. Specifically, NYC launched a Clean Heat program in winter 2008 – 2009 resulting in a 69% decrease in SO_2 concentrations averaged over the city-wide street-level monitoring sites in winter 2012 – 2013 (NYC Health, 2013; https://www1.nyc.gov/assets/doh/downloads/pdf/environmental/air-quality-report-2013.pdf). The Bronx data also reflected the effect of such emission reductions with a 58% decrease in the seasonal median mixing ratio of SO_2 from 9.2 ppbv in winter 2009 to 2.8 ppbv in winter 2015 (Fig. S6). As for NO_2, fuel and mobile combustion emissions comprised >99.5% of the total NO_x emissions in NYC and ~90% over the Eastern US. NYC NO_x emissions changed insignificantly (1%) from 2008 to 2011 and by 15% from 2011 to 2014, while Eastern US mobile and fuel combustion emissions were decreased by 16% and 33%, respectively, from 2008 to 2011, and further decreased by 13% and 9%, respectively, to 2014. These varying changes possibly contributed to confounding the emission signature of GEM vs. NO_x and altered that of GEM vs SO_2.

The effect of local emissions can be accentuated by the correlation between GEM and SO_2 and between GEM and NO_2 for the SO_2 and NO_2 mixing ratios exceeding their respective seasonal 95th percentile concentrations. However, nearly no correlation between GEM and SO_2 as well as between GEM and NO_2 was found in this subset of data (Table 2). It should therefore be cautioned that tracer correlation could not be used to identify source types of GEM or estimate emission ratios of GEM to SO_2 or NO_2 in NYC.

3.5 Regional vs. Local Contributions to NYC Ambient GEM Concentrations

HYSPLIT dispersion simulations were used to obtain a quantitative comparison of the

473 effects of sources outside and inside NYC on NYC ambient concentrations of GEM. As stated
474 in Section 2.3, the modeling domain extended westward to OH and southward to northern VA,
475 and northward to include New England (Fig. 10a), with a total of 522 counties reporting Hg
476 emissions. As described earlier, two scenarios were designed for model simulations:
477 1) With the emission sources in all 522 counties within the domain;
478 2) With the mercury emission sources in all but the five boroughs in NYC.
479 Simulations of Scenario #2 quantifies the contribution of sources outside of NYC to Hg
480 concentrations in NYC, and the difference in the concentrations in NYC between the two
481 scenarios quantifies the contribution of NYC local sources to Hg concentrations in NYC.
482 Shown in Figure 10b is the contribution, in percentage of the total contribution from all
483 anthropogenic emissions in the domain, to NYC ambient concentrations of GEM from
484 anthropogenic emissions alone from local sources, and in Figure 10c is the contribution of
485 emissions from regional anthropogenic sources. There was clearly interannual variability in the
486 contribution of local versus regional anthropogenic sources. Local emissions averaged a
487 contribution of 25% in all winters of 2009 – 2015 with the period minimum of 17% in winter
488 2011 and the maximum of 33% in winter 2013 (Fig. 10b). Conversely, the contribution of
489 regional sources averaged a contribution of 75% in all winters with the largest 83% in winter
490 2011 and the lowest 67% in winter 2013 (Fig. 10c). Compared to that in the winter of the same
491 year, contributions from local sources were larger (by up to 12% in 2009) in summer 2009, 2011,
492 2012, and 2014, close in summer 2010, and 10% smaller in summer 2013 (Fig. 10b).
493 A close examination revealed largely consistent relation between NYC GEM mixing
494 ratios and source contributions. As suggested in Section 3.2, Bronx in winter 2010 experienced
495 the lowest concentrations of GEM in all percentile values, and yet, interestingly the simulated

local contribution in winter 2010 was in the mid-range of the 7 winters. This indicates that the particularly low background concentration in the sweeping northerly flow led to less regional contribution to NYC Hg concentrations than regional sources would in other years. In contrast, winter 2014 saw the highest 25^{th}, 50^{th}, 75^{th}, and 90^{th} percentile concentrations of GEM, and yet the contribution of local sources (~22%) was not even higher than average (25%). As aforementioned, in winter 2014 the Eastern U.S. was most likely under the least dynamic conditions conducive to regional build-up of air pollution, which resulted in a higher than average contribution from regional sources and conversely lower than average contribution from local sources (Fig. 10c). Consistent with GEM, the lower percentile mixing ratios of CO, SO_2, and NO_2 appeared to be elevated or stopped decreasing compared to those in the previous year (Figs. S5,S6).

The HYSPLIT dispersion model simulations suggested that close to three quarters of the anthropogenically induced concentration of GEM in NYC was from regional sources. It should be pointed out that other factors/processes might have competed with the effect of anthropogenic emission reductions, such as legacy and natural emissions, deposition, meteorology, and/or large-scale circulation. Nearly 90% of the model simulation domain is covered by vegetation. SMOKE model output in Ye et al. (2017) suggested that the ratio of anthropogenic to legacy and natural emissions was 0.3 over the domain. Legacy and natural emissions could become dominant under warmer and wetter conditions in summer. Moreover, Hg deposition could be impacted by changes in physical parameters such as light, temperature, and plant species (Rutter et al., 2011). Indeed changes of -30% to 50% in Hg deposition were simulated for the Eastern US from the 2000s to the 2050s due to changes in precipitation (Megaritis et al., 2014). Net GEM surface emissions were estimated to be dominant in summer and net dry deposition in

519 other seasons at majority of AMNet monitoring sites in eastern North America (Zhang et al.,
520 2016). Since Hg deposition and legacy emissions are closely linked, these studies indicate
521 potential changes in legacy emissions in response to variable meteorological conditions and
522 changing climate with subsequent effects on atmospheric Hg concentrations. Therefore, with
523 legacy and natural emissions accounted for, regional contributions to NYC ambient Hg
524 concentrations would be even more dominant.

525 Caution needs to be taken in interpreting the model results due to the limitation of the
526 modeling exercise. First, to save computational time, the simulation domain used in this study
527 was smaller than ideal, and thus with a larger regional domain, the significance of regional
528 anthropogenic sources could be enhanced. Second, the HYSPLIT dispersion model accounts for
529 only long range transport of a pollutant from sources within the domain, without considering
530 chemical transformation, gas-to-particle partitioning, atmosphere-surface exchange of mercury,
531 loss through deposition, and background concentrations. Having said that, for a compound such
532 as GEM with a lifetime of 6 – 12 months, dispersion model simulations would be adequate for
533 providing relative contributions of regional and local sources to ambient concentrations at a
534 location of interest in continental midlatitudes.

535 **4. Summary**

536 For the Bronx site in NYC, distinct annual cycles of GEM were found in 2009 and 2010
537 with higher concentrations in warm than in cool seasons by 10 – 20 ppqv (~10% – 25%),
538 consistent with urban annual cycles reported in the literature. This annual cycle was not
539 reproduced in 2011 with anomalously low concentrations in the warm season and occurred again
540 in 2014. Such temporal variability in the urban GEM concentration was found to be driven by
541 that in large-scale circulation. Seasonal median mixing ratios of GEM was found to be

542 correlated with both the North American TAI and TII in winter and with TII in summer. Further,
543 the intensity and position of the Bermuda High pressure system had a significant impact on
544 Bronx GEM concentrations in warm seasons. Winter 2014 through spring 2015 experienced
545 anomalously strong influence of the Bermuda High resulting in the largest GEM mixing ratios of
546 the entire study period in all percentile values throughout the year. The regional influence on
547 GEM concentrations in Bronx was corroborated by significant, year-round GEM-CO correlation
548 (r up to 0.69, p ~0) over 2008 - 2013. This correlation disappeared or became minimal from
549 winter 2014 through spring 2015 resulting possibly from their very different emission changes in
550 the Eastern U.S.

551 HYSPLIT dispersion model simulations suggested that regional sources outside of NYC
552 contributed to ~75% (67% - 83%) of the anthropogenic portion of the ambient GEM
553 concentration and NYC emissions the remaining ~25% (17% - 33%). Significant interannual
554 variation in the regional and local contributions was found to be consistent with that in large-
555 scale circulation. The fact that there was no clearly defined trend in GEM concentrations at the
556 Bronx site during the study period, despite anthropogenic emission reductions in the Eastern U.S.
557 from 2008 to 2014, suggested that other factors/processes, such as large-scale circulation and
558 legacy/natural emissions, might have dominated over anthropogenic emission reductions.

559 The North Atlantic Subtropical High over 1978 – 2007 had reportedly become more
560 intense, and its western ridge had displaced westward with an enhanced meridional movement
561 (Li et al., 2011). The increasing intensity and spatial extent of the high pressure system could
562 cast a strong influence on the Northeastern US with subsequent effect on ambient concentrations
563 of Hg via regional build-up and changing legacy emissions. This could dominate over the effect
564 of anthropogenic emission reductions, as suggested by this study. Indeed Zhu and Liang (2013)

565 recommended that strong decadal variations in the Bermuda High should be considered in the
566 U.S. air quality dynamic management. Therefore controlling urban ambient concentrations of
567 Hg needs to account for the overall impact of multiple factors, which may not be dominated by
568 emission reductions.

569 **Acknowledgments**

570 This work was funded by the Environmental Protection Agency Grant Agreement
571 #83521501. We are grateful to M. L. Olson and T. R. Bergerhouse of NADP & University of
572 Illinois at Urbana-Champaign and K. Civerolo of NYS DEC for making the Bronx GEM data
573 available. We also thank K. Civerolo for helpful comments and input. The authors gratefully
574 acknowledge the NOAA Air Resources Laboratory for free access to HYSPLIT. The
575 measurement data used in this study could be obtained from AMNet of NADP
576 (http://nadp.sws.uiuc.edu/amn/data.aspx). We greatly appreciate two anonymous reviewers'
577 thoughtful and constructive comments which helped to improve the manuscript significantly.
578 Although this manuscript was reviewed internally, it does not necessarily reflect the views or
579 policies of the NYS DEC.

580 **References**

581 Adler, F. R., and Tanner, C. J.: Urban Ecosystems: Ecological Principles for the Built
582 Environment, 353 pages, Cambridge University Press; 1st edition, 2013.
583 Bradbury, J. A., Keim, B. D., and Wake, C. P.: U.S. East Coast Trough Indices at 500 hPa and
584 New England Winter Climate Variability, J. Clim., 15, 3509-3517, 2002.
585 Brown, R. J. C., Goddard, S. L., Butterfield, D. M., Brown, A. S., Robins, C., Mustoe, C. L., and
586 McGhee, E. A.: Ten years of mercury measurement at urban and industrial air quality
587 monitoring stations in the UK, Atmos. Environ., 109, 1-8, 2015.

588 Chen, L., M. Liu, Z. Xu, R. Fan, J. Tao, D. Chen, D. Zhang, D. Xie, and J. Sun: Variation trends
589 and influencing factors of total gaseous mercury in the Pearl River Delta - A highly
590 industrialized region in South China influenced by seasonal monsoons, Atmos. Environ., 77,
591 757-766, 2013.
592 Cheng, I., Lu, J., and Song, X.: Studies of potential sources that contributed to atmospheric
593 mercury in Toronto, Canada, Atmos. Environ., 43, 6145–6158, 2009.
594 Choi, H., Huang, J., Mondal, S., and Holsen, T. M.: Variation in concentrations of three mercury
595 (Hg) forms at a rural and a suburban site in New York State, Sci. Total Environ., 448, 96-
596 106. doi:10.1016/j.scitotend.2012.08.052, 2013.
597 Civerolo, K. L., Rattigan, O. V., Felton, D. H., Hirsch, M. J., and DeSantis, S.: Mercury wet
598 deposition and speciated air concentrations from two urban sites in New York State;
599 temporal patterns and regional context, Aeros. Air Qual. Res.,
600 doi:10.4209/aaqr.2014.03.0052, 2014.
601 Denis, M. S., Song, X., Lu, J. Y., and Feng, X.: Atmospheric gaseous elemental mercury in
602 downtown Toronto, Atmos. Environ., 40(21), 4016-4024,
603 doi:10.1016/j.atmosenv.2005.07.078, 2006.
604 Draxler, R. R. (1999), HYSPLIT4 user's guide, NOAA Tech. Memo. ERL ARL-230, NOAA Air
605 Resources Laboratory, Silver Spring, MD.
606 Draxler, R. R., and Hess, G. D.: An overview of the HYSPLIT_4 modeling system of
607 trajectories, dispersion, and deposition, Aust. Meteor. Mag., 47, 295-308, 1998.
608 Draxler, R. R., and Hess, G. D.: Description of the HYSPLIT_4 modeling system, NOAA Tech.
609 Memo. ERL ARL-224, NOAA Air Resources Laboratory, Silver Spring, MD, 24 pp, 1997.
610 Driscoll, C. T., Mason, R. P., Chan, H. M., Jacob, D. J., and Pirrone, N.: Mercury as a global

611 pollutant: sources, pathways, and effect, Environ. Sci. Technol., 47, 4967–4983, 2013.
612 Engle, M. A., Tate, M. T., Krabbenhoft, D. P., Schauer, J. J., Kolker, A., Shanley, J. B., and
613 Bothner, M. H.: Comparison of atmospheric mercury speciation and deposition at nine sites
614 across central and eastern North America, J. Geophys. Res.-Atmos., 115,
615 doi:10.1029/2010JD014064, 2010.
616 Fang, F., Wang, Q., and Li, J.: Urban environmental mercury in Changchun, a metropolitan city
617 in Northeastern China: source, cycle, and fate, Sci. Total Environ., 330, 159 – 170, 2004.
618 Feng, X., Tang, S., Shang, L., Yan, H., Sommar, J., and Lindqvist, O.: Total gaseous mercury in
619 the atmosphere of Guiyang, P. R. China, Sci. Total Environ., 304, 61 – 72, 2003.
620 Fu, X. W., Zhang, H., Yu, B.,Wang, X., Lin, C.-J., and Feng, X. B.: Observations of atmospheric
621 mercury in China: a critical review, Atmos. Chem. Phys., 15, 9455–9476, doi:10.5194/acp-
622 15-9455-2015, 2015.
623 Gabriel, M. C., Williamson, D. G., Brooks, S., and Lindberg, S.: Atmospheric speciation of
624 mercury in two contrasting Southeastern US airsheds, Atmos. Environ., 39, 4947–4958,
625 2005.
626 Gay, D. A., Schmeltz, D., Prestbo, E., Olson, M., Sharac, T. and Tordon, R.: The Atmospheric
627 Mercury Network: Measurement and Initial Examination of an Ongoing Atmospheric
628 Mercury Record across North America, Atmos. Chem. Phys., 13, 11339–11349, 2013.
629 Hall, C. B., Mao, H., Ye, Z., Talbot, R., Ding, A., Zhang, Y., Zhu, J., Wang, T., Lin, C. J., Fu,
630 C., and Yang, X.: Sources and dynamic processes controlling background and peak
631 concentrations of TGM in Nanjing, China, Atmosphere, 5(1), 124-155, 2014.

632 Jen, Y.-H., Yuan, C.-S., Hung, C.-H., Ie, I.-R., and Tsai, C.-M.: Tempospatial Variation and
633 Partition of Atmospheric Mercury during Wet and Dry Seasons at Sensitivity Sites within a
634 Heavily Polluted Industrial City, Aeros. Air Quality Res., 13, 13-23, 2013
635 Kim, K. H., and Kim, M. Y.: The temporal distribution characteristics of total gaseous mercury
636 at an urban monitoring site in Seoul during 1999–2000, Atmos. Environ., 35, 4253–4263,
637 2001.
638 Kim, K. H., Yoon, H. O., Brown, R. J., Jeon, E. C., Sohn, J. R., Jung, K., Park, C. G., and Kim,
639 I. S.: Simultaneous monitoring of total gaseous mercury at four urban monitoring stations in
640 Seoul, Korea, Atmos. Res., 132, 199-208, 2013.
641 Kim, K.-H., Brown, R. J., Kwon, E., Kim, I.-S., and Sohn, J.-R.: Atmospheric mercury at an
642 urban station in Korea across three decades, Atmos. Environ., 131, 124-132, 2016.
643 Landis, M. S., Stevens, R. K., Schaedlich, F. and Prestbo, E. M.: Development and
644 Characterization of an Annular Denuder Methodology for the Measurement of Divalent
645 Inorganic Reactive Gaseous Mercury in Ambient Air. Environ. Sci. Technol., 36, 3000–
646 3009, 2002.
647 Lan, X., Talbot, R., Castro, M., Perry, K., and Luke, W.: Seasonal and diurnal variations of
648 atmospheric mercury across the US determined from AMNet monitoring data, Atmos. Chem.
649 Phy., 12(4), 10569-10582. doi:10.5194/acp-12-10569-2012, 2012.
650 Lan, X., Talbot, R., Laine, P., Lefer, B., Flynn, J., and Torres, A.: Seasonal and diurnal
651 variations of total gaseous mercury in urban Houston, TX, USA, Atmosphere, 5, 399–419,
652 2014.
653 Li, W., Li, L., Fu, R., Deng, Y., and Wang, H.: Changes to the North Atlantic Subtropical High
654 and Its Role in the Intensification of Summer Rainfall Variability in the Southeastern United

States, J. Clim., 24(5), 1499-1506, 2011.

Lindberg, S., Bullock, R., Ebinghaus, R., Engstrom, D., Feng, X., Fitzgerald, W., Pirrone, N., Prestbo, E., and Seigneur, C.: A synthesis of progress and uncertainties in attributing the sources of mercury in deposition, *Ambio, 36*(1), 19-32, 2007.

Lindberg, S. E., and Stratton, W. J.: Atmospheric mercury speciation: concentrations and behavior of reactive gaseous mercury in ambient air, Environ. Sci. Technol., 32, 49–57, 1998.

Liu, B., Keeler, G. J., Dvonch, J. T., Barres, J. A., Lynam, M. M., Marsik, F. J., and Morgan, J. T.: Temporal variability of mercury speciation in urban air, Atmos. Environ., 41(9), 1911-1923. doi:10.1016/j.atmosenv.2006.10.063, 2007.

Liu, B., Keeler, G. J., Dvonch, J. T., Barres, J. A., Lynam, M. M., Marsik, F. J., and Morgan, J. T.: Urban-rural differences in atmospheric mercury speciation, Atmos., Environ., 44, 2013-2023, 2010.

Lyman, S. N., and Gustin, M. S.: Determinants of atmospheric mercury concentrations in Reno, Nevada, USA, Sci. Total Environ., 408(2), 431-438, 2009.

Lombard, M. A. S., Bryce, J., Mao, H., and Talbot, R.: Mercury deposition in southern New Hampshire, 2006 - 2009, Atmos. Chem. Phys., 11, 7657–7668, www.atmos-chem-phys.net/11/7657/2011/doi:10.5194/acp-11-7657-2011, 2011.

Mao, H., Talbot, R., Sigler, J. M., Sive, B. C., and Hegarty, J. D.: Seasonal and diurnal variation in Hg° over New England, Atmos. Chem. Phys., 8, 1403-1421, 2008.

Mao, H., and Talbot, R.: Long-term variation in speciated mercury at marine, coastal and inland sites in New England: Part I Temporal Variability, Atmos. Chem. Phys.,12, 5099-5112, doi:10.5194/acp-12-5099-2012, 2012.

678 Mao, H., Cheng, I., and Zhang, L.: Current understanding of the driving mechanisms for
679 spatiotemporal variations of atmospheric speciated mercury: a review, Atmos. Chem. Phy.,
680 16, 1–28, 2016, www.atmos-chem-phys.net/16/1/2016/, doi:10.5194/acp-16-1-2016, 2016.
681 Megaritis, A. G., Murphy, B. N., Racherla, P. N., Adams, P. J., Pandis, S. N., Impact of climate
682 change on mercury concentrations and deposition in the eastern United States, Sci. Total
683 Environ. , 487, 299-312, doi: 10.1016/j.scitotenv.2014.03.084, 2014.
684 Nair, U. S., Wu, Y., Walters, J., Jansen, J., Edgerton, E. S.: Diurnal and seasonal variation of
685 mercury species at coastal-suburban, urban, and rural sites in the southeastern United States,
686 Atmos. Environ., 47, 499-508, 2012.
687 Peterson, C., Gustin, M., and Lyman, S.: Atmospheric mercury concentrations and speciation
688 measures from 2004 to 2007 in Reno, Nevada, USA, Atmos. Environ., 43(30), 4646-4654.
689 doi:10.1016/j.atmosenv.2009.04.053, 2009.
690 Rutter, A. P., Schauer, J. J., Shafer, M. M., Creswell, J., Olson, M. R., Clary, A., Robinson, M.,
691 Parman, A. M., and Katzman, T. L.: Climate Sensitivity of Gaseous Elemental Mercury Dry
692 Deposition to Plants: Impacts of Temperature, Light Intensity, and Plant Species, Environ.
693 Sci. Technol., 45(2), 569-575, 2011.
694 Selin, N. E.: Global change and mercury cycling: Challenges for implementing a global mercury
695 treaty, Environ. Toxicol. Chem., 33, 6, 1202–1210, 2014.
696 Seo, Y.-S., et al.: Characteristics of total gaseous mercury (TGM) concentrations in an industrial
697 complex in South Korea: impacts from local sources, Atmos. Chem. Phys., 16, 10215–
698 10228, 2016.
699 Sigler, J. M., Mao, H., and Talbot, R.: Gaseous elemental and reactive mercury in southern New
700 Hampshire, Atmos. Chem. Phys., 9, 1929-1942, 2009.

701 Sprovieri, F., Pirrone, N., Ebinghaus, R., Kock, H., and Dommergue, A.: A review of worldwide
702 atmospheric mercury measurements, Atmos. Chem. Phys., 10(17), 8245-8265.
703 doi:10.5194/acp-10-8245-2010, 2010.
704 Stamenkovic, J., Lyman, S., and Gustin, M. S.: Seasonal and diel variation of atmospheric
705 mercury concentrations in the Reno (Nevada, USA) airshed, Atmos. Environ., 41, 6662–
706 6672, 2007.
707 Stein, A. F., Draxler, R. R., Rolph, G. D., Stunder, B. J. B., Cohen, M. D., and Ngan, F.:
708 NOAA's HYSPLIT atmospheric transport and dispersion modeling system, Bull. Amer.
709 Meteor. Soc., 96, 2059-2077, http://dx.doi.org/10.1175/BAMS-D-14-00110.1, 2015.
710 Wang, Y., Huang, J., Hopke, P. K., Holsen, T. M., Rattigan, O. V., Chalupa, D. C., and Utell, M.
711 J.: Effect of the shutdown of a large coal-fired power plant on ambient mercury species,
712 Chemosphere, 92, 360–367, 2013.
713 Xu, X., Akhtar, U., Clark, K., and Wang, X.: Temporal Variability of Atmospheric Total
714 Gaseous Mercury in Windsor, ON, Canada, Atmosphere, 5, 536-556,
715 doi:10.3390/atmos5030536, 2014.
716 Ye, Z., Mao, H., Hogrefe, C., Zhang, Y., and Jaegle, L.: Regional photochemical model
717 evaluation of speciated ambient mercury and mercury wet and dry deposition, to be
718 submitted to J. Adv. Model. Earth Sys. , 2017.
719 Zhang, L., Wang, S., Wang, L. and Hao, J. M.: Atmospheric mercury concentration and
720 chemical speciation at a rural site in Beijing, China: Implications of mercury emission
721 sources*., Atmos. Chem. Phys., 13*(20), 10505-10516. doi:10.5194/acp-13-10505-2013, 2013.
722 Zhang, L., et al.: The estimated six-year mercury dry deposition across North America, Environ.
723 Sci. Technol., doi: 10.1021/acs.est.6b04276, 50, 12864-12873, 2016.

Zhou, Y., **H. Mao**, K. Demerjian, C. Hogrefe, and J. Liu**:** Regional and Hemispheric Influences on Temporal Variability in Baseline Carbon Monoxide and Ozone over the Northeast US, *Atmos. Environ.*, 164, 309-324, 2017.

Zhou, H., Zhou, C., Lynam, M. M., Dvonch, J. T., Barres, James A., Hopke, P. K., Cohen, M., Holsen, T. M.: Atmospheric Mercury Temporal Trends in the Northeastern United States from 1992 to 2014: Are Measured Concentrations Responding to Decreasing Regional Emissions? Environ. Sci. Technol. Lett., 4, 91−97, 2017. DOI: 10.1021/acs.estlett.6b00452.

Zhu, J., Wang, T., Talbot, R., Mao, H., Hall, C. B., Yang, X., and Huang, X.: Characteristics of atmospheric total gaseous mercury (TGM) observed in urban Nanjing, China, Atmos. Chem. Phy., 12(24), 12103, doi:10.5194/acp-12-12103-2012, 2012.

Zhu, J., and Liang, X.-Z.: Impacts of the Bermuda High on Regional Climate and Ozone over the United States, J. Clim., 26, 1018-1026, 2013.

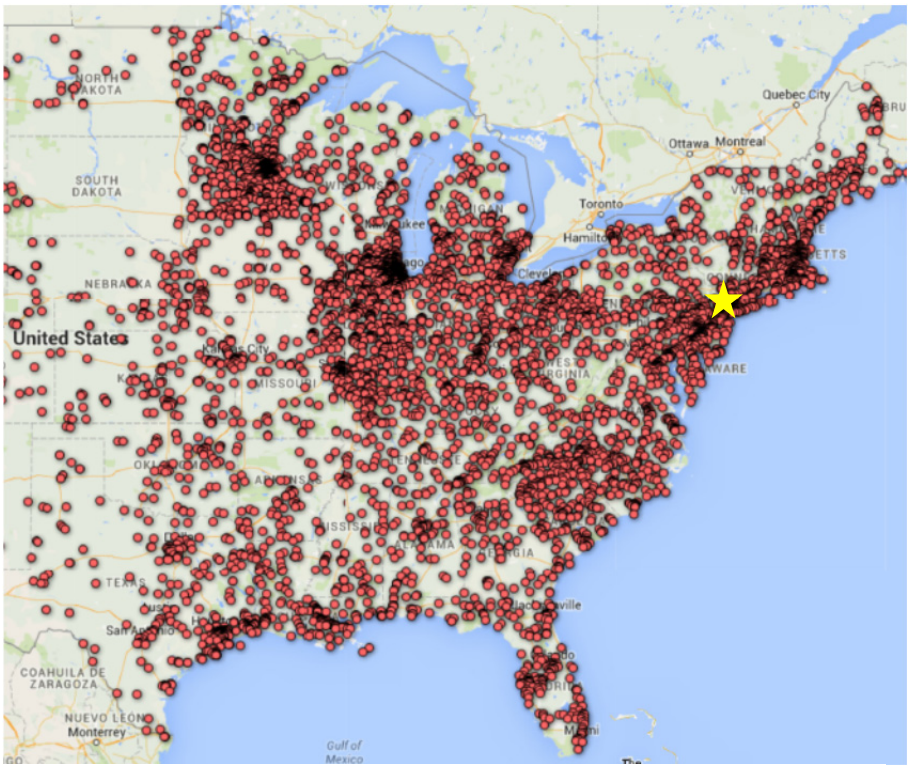

Figure 1. Map of mercury emission sources in the Eastern US. The yellow asterisk marks the location of the Bronx site.

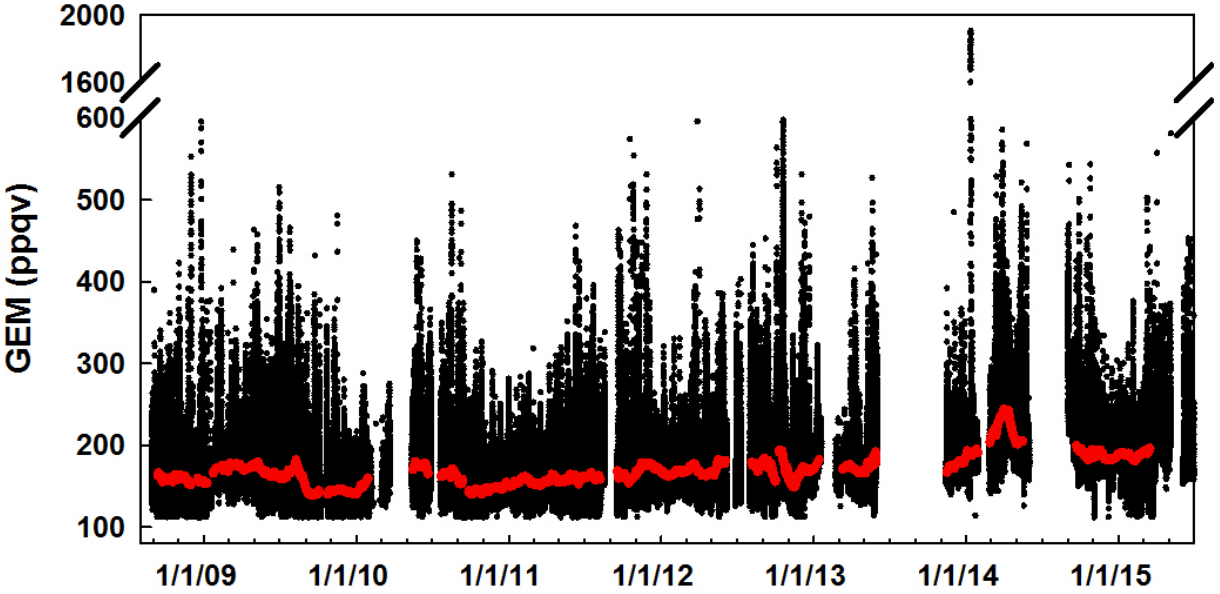

Figure 2. Time series of 5-min average GEM mixing ratios (black dots) with 30-day running average (red line) during the study period.

202

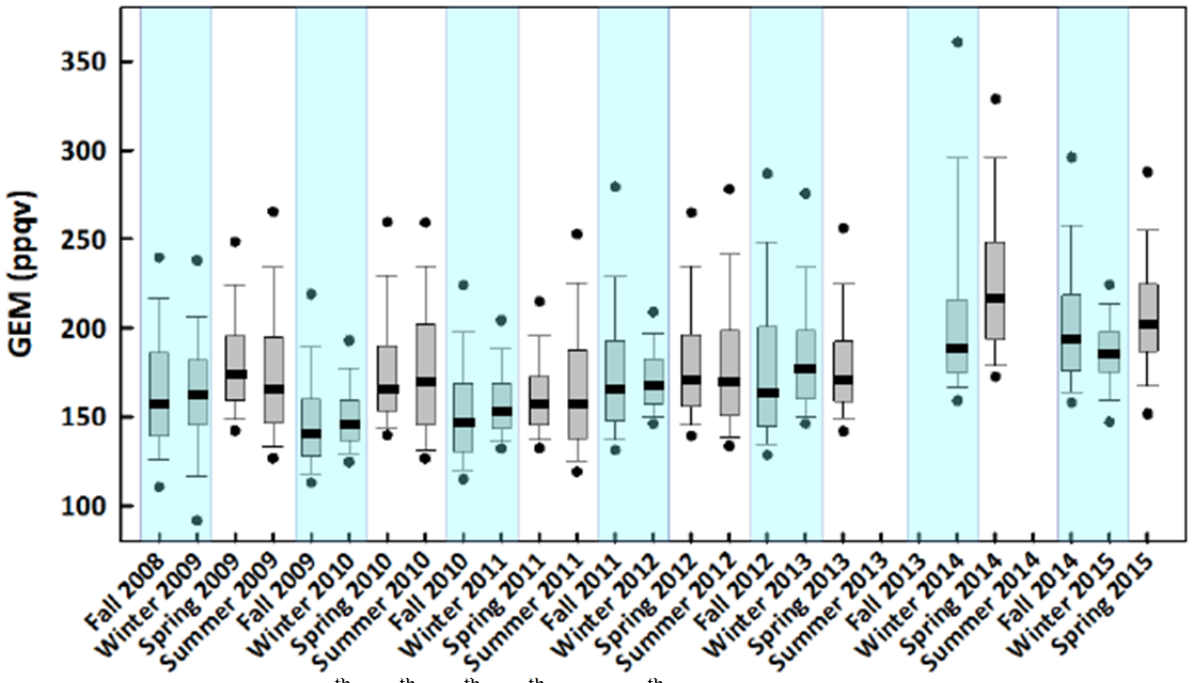

Figure 3. Seasonal 10th, 25th, 50th, 75th, and 90th GEM percentile values. The black dots represent the 5th and 95th percentile value. The thickened lines represent median values. The blue shaded areas are the cool season including fall and the following winter.

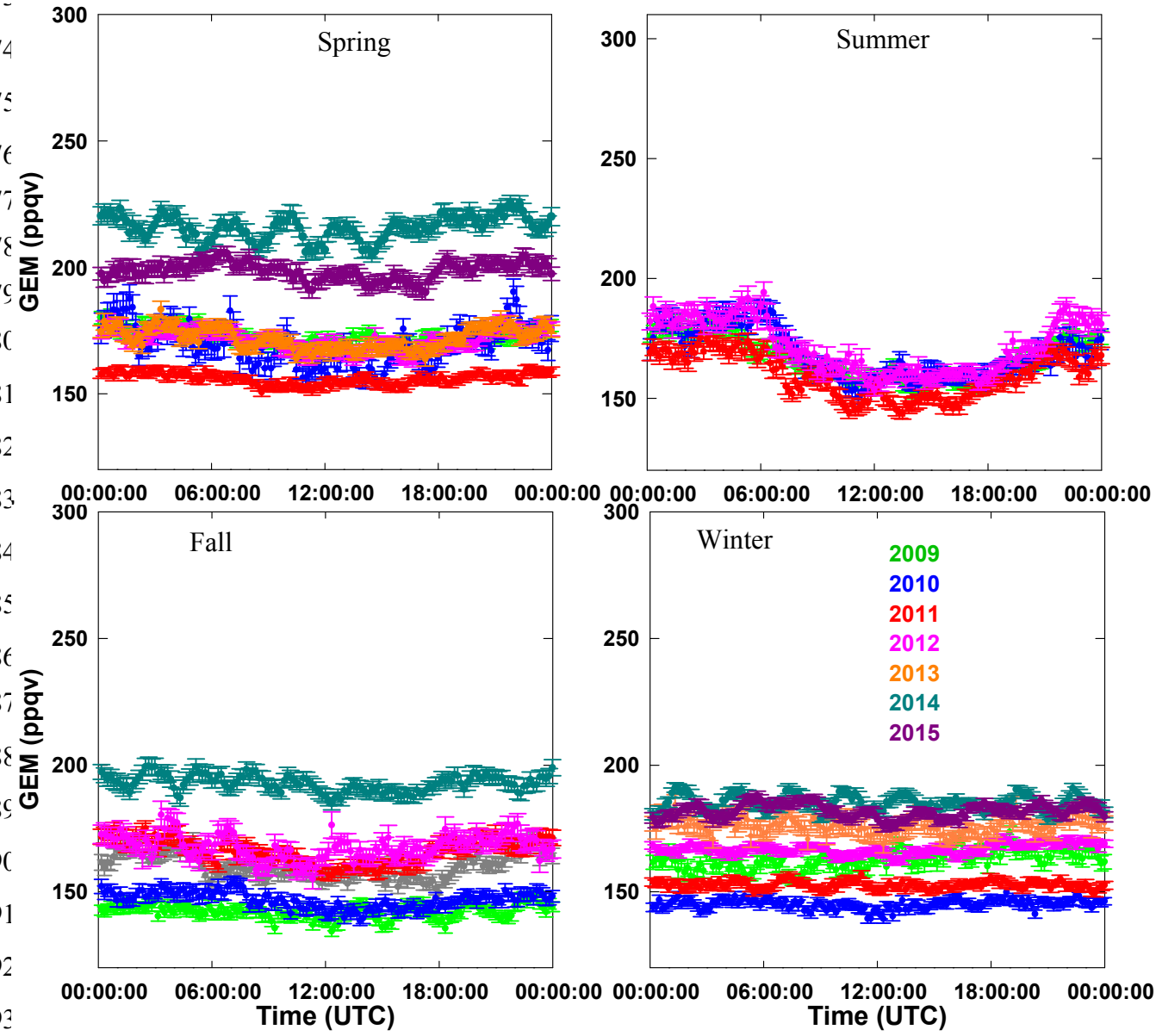

Figure 4. Seasonal averaged diurnal cycles of GEM for spring, summer, fall, and winter.

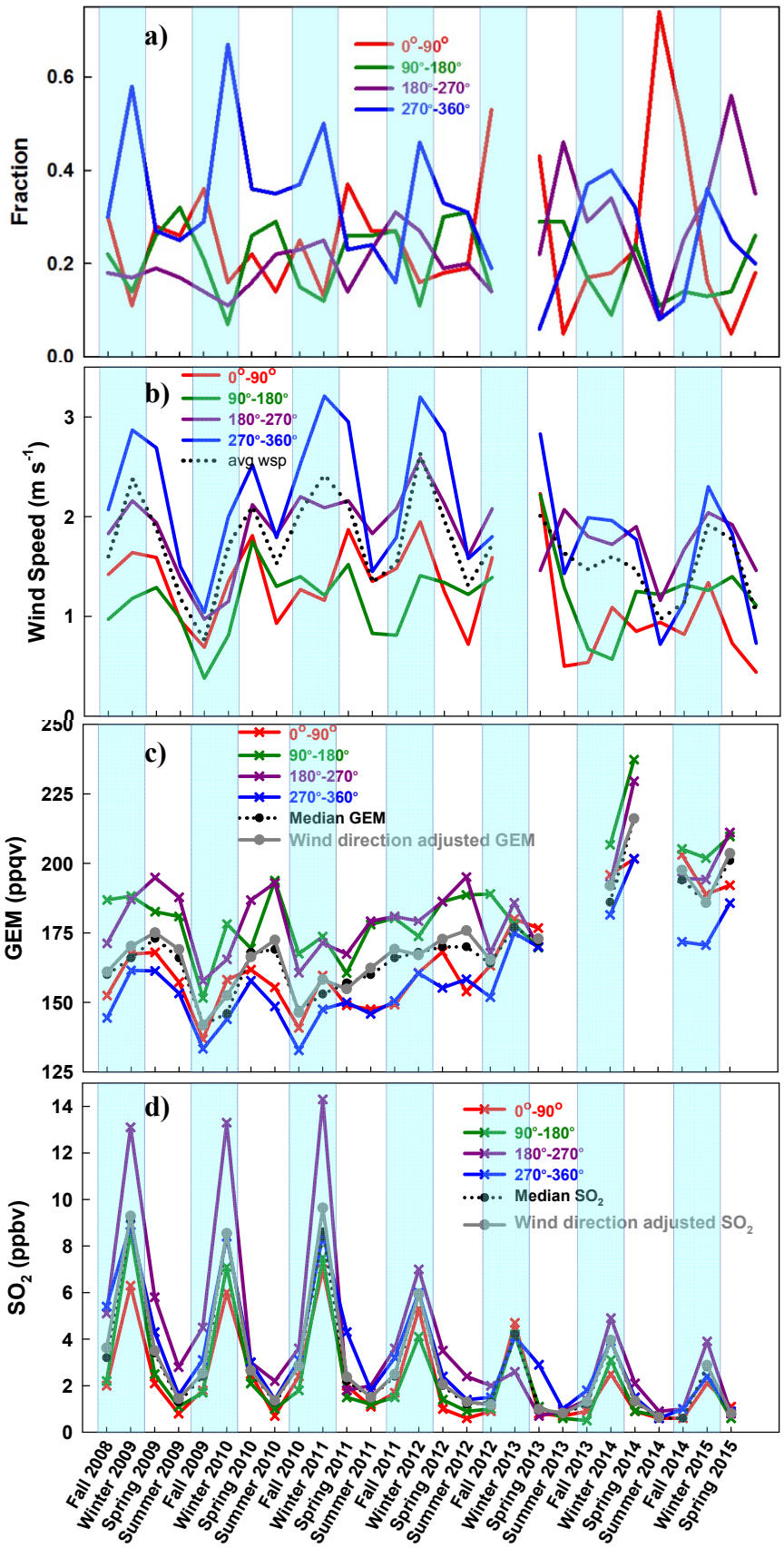

Figure 5. a) Fraction of wind coming from, b) wind speed, c) GEM and d) SO_2 averaged in the four wind quadrants in each season together with seasonal median and wind direction adjusted values. The shaded areas indicate the cool seasons. In b) the black dotted line indicates the wind speed averaged in all directions. In c) and d) the black dotted line and black solid dots represent the overall seasonal median values of GEM and SO_2, and the dark grey dotted line and dark grey solid dots for the wind direction adjusted GEM and SO_2 values.

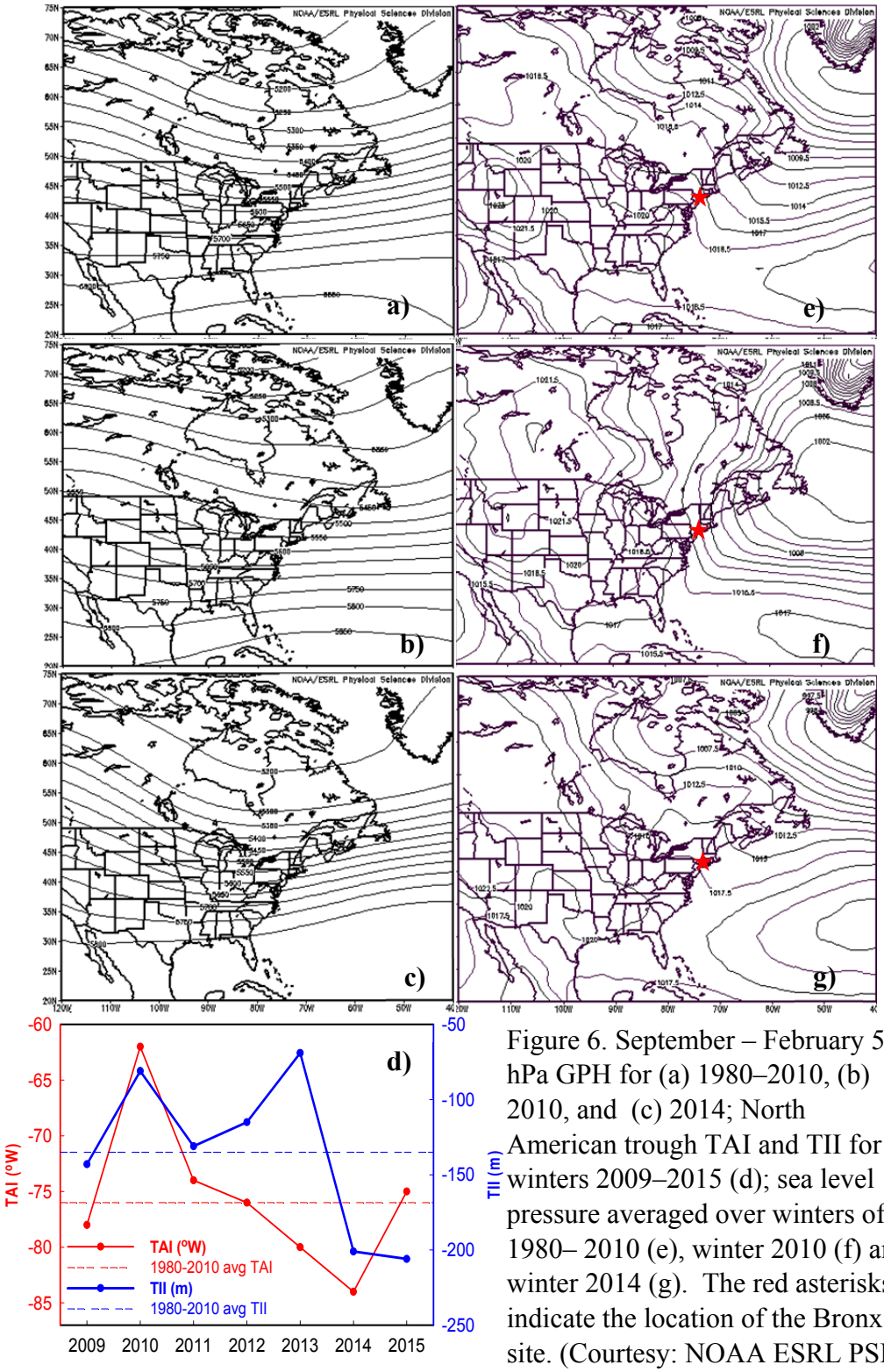

Figure 6. September – February 500 hPa GPH for (a) 1980–2010, (b) 2010, and (c) 2014; North American trough TAI and TII for winters 2009–2015 (d); sea level pressure averaged over winters of 1980– 2010 (e), winter 2010 (f) and winter 2014 (g). The red asterisks indicate the location of the Bronx site. (Courtesy: NOAA ESRL PSD Interactive Climate Analysis).

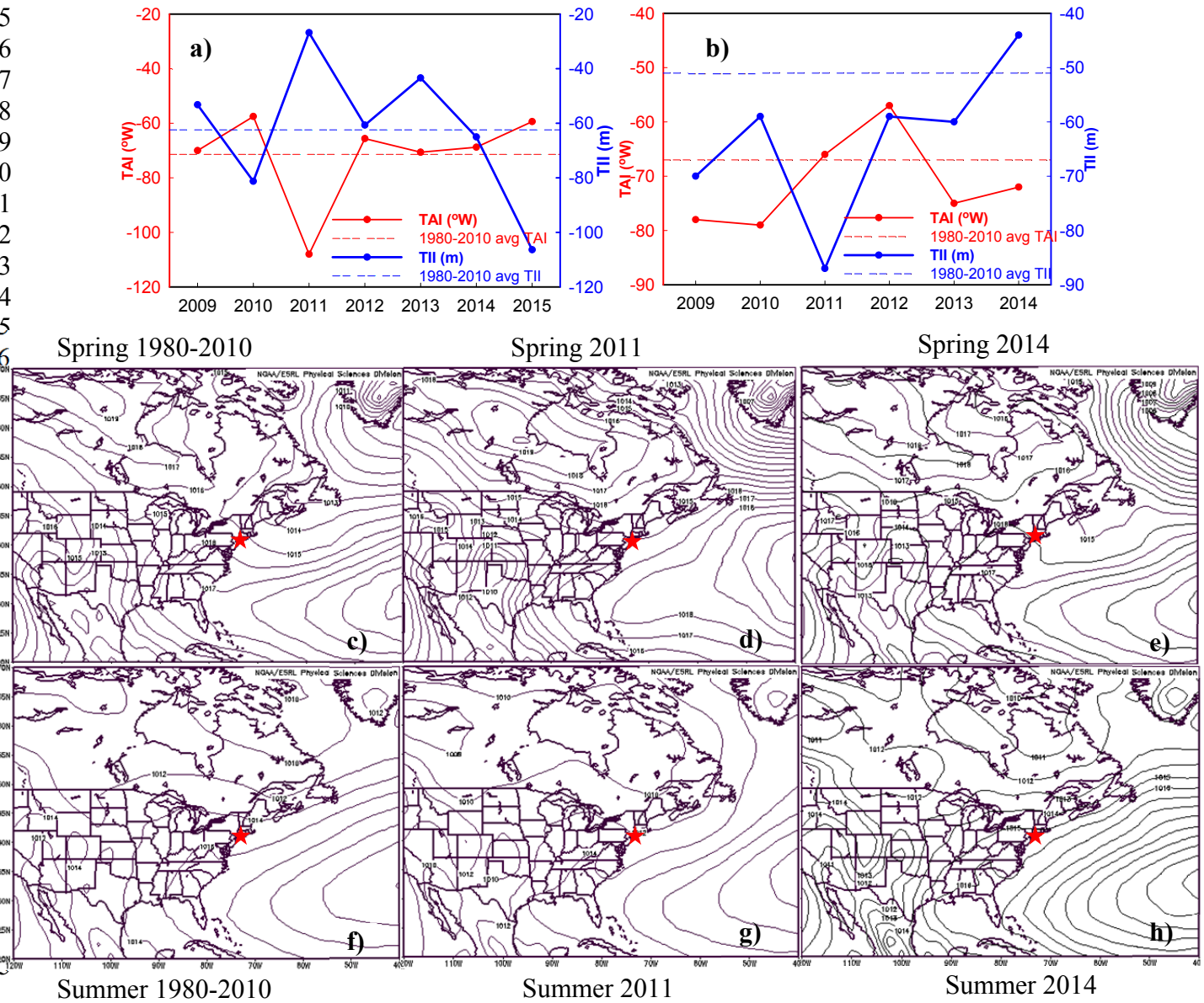

Figure 7. The axis position (TAI) and intensity (TII) of the 500 hPa North American Trough in spring (a) and summer (b). Sea level pressure (SLP) in spring (c) 1980-2010, (d) 2011, and (e) 2014. SLP in summer (f) 1980 – 2010, (g) 2011, and (h) 2014. The red asterisks indicate the Bronx site location. (Courtesy: NOAA ESRL PSD Interactive Climate Analysis)

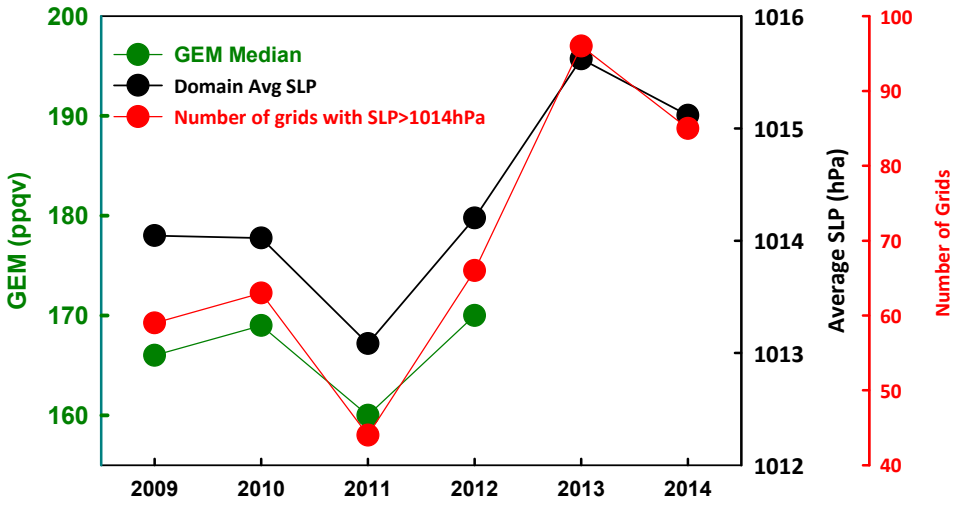

Figure 8. Average sea level pressure (SLP) over the domain of 25°N-50°N, 95°W-70°W (black), number of grids with SLP >1014 hPa (red), and seasonal median GEM mixing ratios (dark green) in the summer.

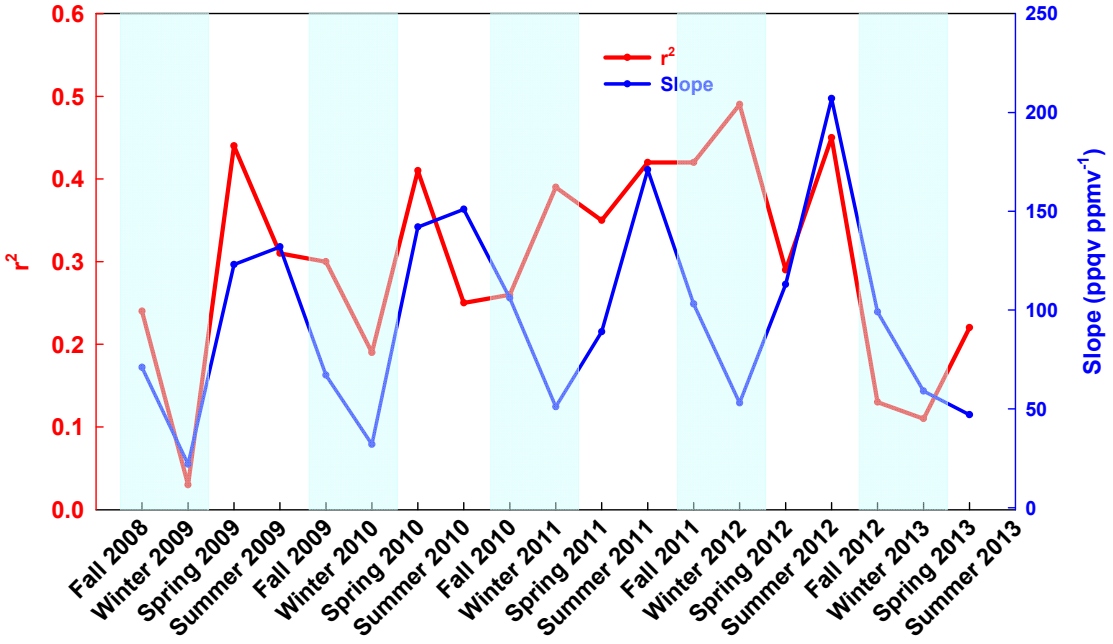

Figure 9. Values of r^2 (red) and slope (blue) of GEM-CO correlation during each season from 2008 to 2013. All r^2 values were statistically significant with *p* approaching 0.

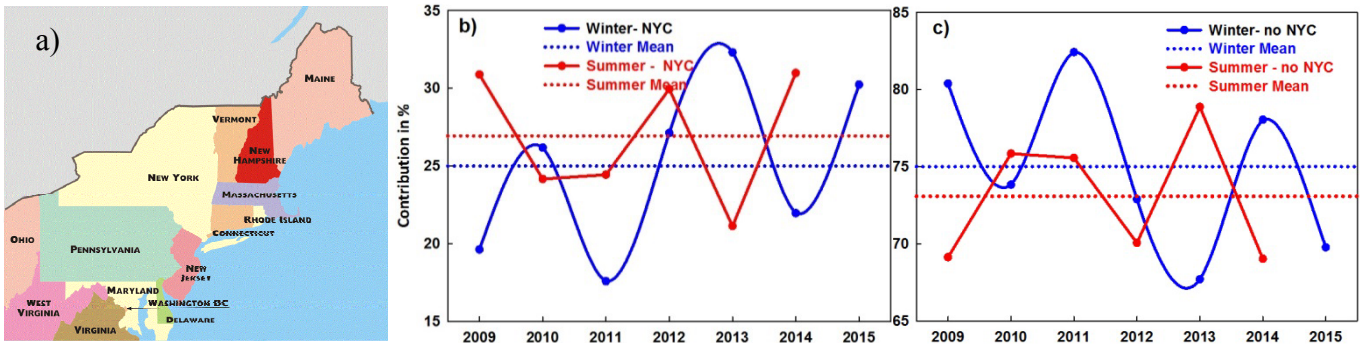

Figure 10. a) Counties and states that contributed to Hg in NYC; b) Contributions (in %) of NYC sources to NYC Hg concentrations; c) Contributions (in %) of sources outside of NYC to NYC Hg concentrations in winter (blue) and summer (red).

Table 1. Seasonal 10th, 25th, 75th, and 90th percentile and median mixing ratios as well as the range of GEM from the Bronx site. Sample numbers are indicated with "Sample #". "Frequency of higher values" represents the warm/cold seasonal frequency of GEM exceeding the 75th percentile mixing ratio (200 ppqv) of all data.

		10th	25th	Median	75th	90th	Range	Sample #	Frequency of high values
2008	Fall	132	142	160	187	217	112-552	13677	14%
2009	Winter	135	151	166	184	207	112-62	8728	
	Spring	149	159	173	196	224	112-463	14655	22%
	Summer	134	147	166	195	234	112-515	14986	
	Fall	121	130	142	161	191	112-461	12113	6%
2010	Winter	129	137	146	159	177	112-288	9749	
	Spring	144	153	168	191	229	114-450	4203	24%
	Summer	132	145	169	202	234	112-531	9014	
	Fall	122	132	147	169	197	112-1581	11407	7%
2011	Winter	136	143	153	169	188	112-318	15085	
	Spring	137	145	157	172	195	112-352	15419	12%
	Summer	127	139	160	188	226	112-468	11522	
	Fall	138	148	166	193	228	112-660	12758	13%
2012	Winter	150	157	168	182	197	119-375	15117	
	Spring	145	156	170	195	234	112-1516	13708	23%
	Summer	140	152	170	199	243	112-445	8174	
	Fall	134	142	157	190	246	11-896	13210	25%
2013	Winter	151	160	177	199	234	112-1068	7781	
	Spring	149	159	172	193	225	14-527	12040	20%
	Summer	-	-	-	-	-	-	-	-
	Fall	-	-	-	-	-	-	-	-
2014	Winter	168	174	186	201	228	114-1908	10986	26%
	Spring	179	194	216	248	296	126-1151	15272	67%
	Summer	-	-	-	-	-	-	-	-
	Fall	164	176	194	219	258	112-543	12828	31%
2015	Winter	159	176	186	198	214	112-376	15218	
	Spring	168	187	201	225	255	112-687	11107	52%
	2008-2015	138	152	173	**200**	239	112-1908	309833	

Table 2. Pearson correlation coefficients (r) between GEM and SO_2 and between GEM and NO_2 with *p* values in parenthesis, for seasons during fall 2008 - spring 2015.

	All data		SO_2&NO_2 for GEM> 95th percentile	
	SO_2	NO_2	SO_2	NO_2
Fall 2008	-0.02 (=0.371)	0.32 (<0.0001)	0.07 (=0.502)	-0.08 (=0.476)
Winter 2009	0.26 (<0.0001)	0.41 (<0.0001)	-0.20 (=0.132)	-0.02 (=0.875)
Spring 2009	0.01 (=0.608)	0.05 (=0.03)	-0.02 (=0.832)	0.09 (=0.41)
Summer 2009	0.16 (<0.0001)	0.46 (<0.0001)	0.50 (<0.0001)	0.25 (=0.0152)
Fall 2009	0.25 (<0.0001)	0.53 (<0.0001)	0.08 (=0.505)	0.15 (=0.190)
Winter 2010	0.42 (<0.0001)	0.55 (<0.0001)	0.03 (=0.794)	0.05 (=0.693)
Spring 2010	0.07 (=0.094)	0.38 (<0.0001)	-0.13 (=0.507)	0.13 (=0.505)
Summer 2010	0.10 (<0.0001)	0.45 (<0.0001)	-0.07 (=0.605)	0.22 (=0.105)
Fall 2010	0.06 (=0.0101)	0.36 (<0.0001)	0.09 (=0.403)	0.00 (=0.972)
Winter 2011	0.51 (<0.0001)	0.71 (<0.0001)	-0.20 (=0.0464)	-0.03 (=0.802)
Spring 2011	0.01 (=0.761)	0.41 (<0.0001)	0.01 (=0.901)	0.24 (=0.0156)
Summer 2011	0.14 (<0.0001)	0.53 (<0.0001)	-0.12 (=0.285)	0.11 (=0.296)
Fall 2011	0.22 (<0.0001)	0.51 (<0.0001)	0.34 (=0.0018)	0.26 (=0.0185)
Winter 2012	0.20 (<0.0001)	0.57 (<0.0001)	0.00 (=0.986)	0.27 (=0.0078)
Spring 2012	0.13 (<0.0001)	0.44 (<0.0001)	-0.12 (=0.268)	-0.16 (=0.125)
Summer 2012	0.29 (<0.0001)	0.49 (<0.0001)	-0.10 (=0.475)	0.02 (=0.903)
Fall 2012	-0.15 (<0.0001)	0.13 (<0.0001)	-0.43 (<0.0001)	-0.46 (<0.0001)
Winter 2013	0.10 (=0.0016)	0.37 (<0.0001)	-0.23 (=0.101)	-0.31 (=0.0196)
Spring 2013	N/A	N/A	N/A	N/A
Summer 2013	N/A	N/A	N/A	N/A
Fall 2013	N/A	N/A	N/A	N/A
Winter 2014	-0.12 (<0.0001)	0.04 (=0.13)	-0.47 (<0.0001)	0.21 (=0.0944)
Spring 2014	0.07 (=0.003)	0.39 (<0.0001)	0.05 (=0.608)	0.05 (=0.654)
Summer 2014	N/A	N/A	N/A	N/A
Fall 2014	-0.13 (<0.0001)	0.33 (<0.0001)	0.11 (=0.362)	0.02 (=0.887)
Winter 2015	0.27 (<0.0001)	0.60 (<0.0001)	-0.07 (=0.570)	-0.07 (=0.555)
Spring 2015	0.13 (<0.0001)	0.52 (<0.0001)	0.05 (=0.656)	0.07 (=0.557)